Connection between coherent phonons and electron-phonon coupling in Sb (111)

S. Sakamoto ●,[1,*] N. Gauthier ●,[1] P. S. Kirchmann ●,[1] J. A. Sobota ●,[1,†] and Z.-X. Shen ●[1,2]

[1]*Stanford Institute for Materials and Energy Sciences, SLAC National Accelerator Laboratory,*
2575 Sand Hill Road, Menlo Park, California 94025, USA
[2]*Geballe Laboratory for Advanced Materials, Department of Physics and Applied Physics,*
Stanford University, Stanford, California 94305, USA

We report time- and angle-resolved photoemission spectroscopy (trARPES) measurements on the Sb(111) surface. We observe band- and momentum-dependent binding-energy oscillations in the bulk and surface bands driven by A_{1g} and E_g coherent phonons. While the bulk band shows simultaneous A_{1g} and E_g oscillations, the surface bands show either A_{1g} or E_g oscillations. The observed behavior is reproduced by frozen-phonon calculations based on density functional theory. This evidences the connection between electron-phonon coupling and coherent binding-energy dynamics tied to lattice vibration and confirms that band-, momentum-, and mode-dependent electron-phonon coupling can indeed be probed by trARPES in the low fluence limit.

DOI: 10.1103/PhysRevB.105.L161107

In recent years, there has been growing interest in using nonequilibrium techniques to probe equilibrium material properties. Coherent phonons, which are nonequilibrium atomic motions driven by an ultrafast light pulse, are particularly useful for this purpose since the oscillatory displacements of the atoms are associated with simultaneous oscillations in the electronic binding energies. As a result, the lattice and electronic dynamics associated with coherent phonons provide direct information on the equilibrium property of electron-phonon coupling [1,2].

Time- and angle-resolved photoemission spectroscopy (trARPES) is one of the most powerful methods to study coherent phonons, as it can directly monitor the temporal evolution of electronic band structure. Specifically, it can resolve $\Delta\varepsilon_n(k)$, the electronic energy shift as a function of band index n and electron momentum k, separately for each phonon mode via Fourier analysis of its oscillatory behavior. This is proportional to the deformation potential $D_n(k) = \Delta\varepsilon_n(k)/\Delta r$, where Δr is the corresponding lattice distortion, which represents the strength of electron-phonon coupling with n-, k-, and mode-specificity [1]. This technique has been applied to deduce the behavior of electron-phonon coupling in materials with surface states [3–6], strong electron correlations [7–9], coexisting phases [10], and complex multiband electronic structures [11]. Integration with ultrafast structural probes to measure Δr enables theory-free quantification of the deformation potential [7,8].

As trARPES investigations of coherent phonons advance toward increasingly complex material systems, it is critical to verify that the nonequilibrium probe is faithful to the equilibrium quantity of interest, especially since deviations

from expected behavior are taken as evidence of nontrivial physics [8]. Indeed, coherent phonons are generated by complex time-dependent light-induced forces, which quickly decay through electron-phonon interactions [12,13], so it is unclear whether the resultant oscillation of valence electron states is described by the near-equilibrium deformation potential. trARPES experiments on semimetals and topological insulators have shown that frozen-phonon density functional theory (DFT) calculations provide an adequate description of the band [4] and k dependence [3,6] of binding-energy dynamics attributed to fully symmetric A_{1g} coherent phonons. It is desirable to extend this analysis to modes of different symmetries, preferably in a system which exhibits a band- and k-dependent response, to establish a comprehensive benchmark across the parameter space relevant to electron-phonon coupling in complex materials.

Sb is an ideal material for such a study. Sb is a topological semimetal [14–16] with bulk and surface bands well described by DFT [17] and accessible by photoemission with laser sources [18]. Sb has a rhombohedral A7 crystal structure [Fig. 1(a)], which is a cubic lattice distorted along the (111) direction (or the c axis direction in a hexagonal representation). The distortion happens due to a Peierls instability along the (111) direction, and Sb atoms form honeycomblike bilayers. This structure hosts a total of two optical phonon modes (A_{1g} and E_g), both of which are susceptible to coherent excitation [19,20] and the mechanism of which has been studied intensively [21–25].

In this letter, we report trARPES measurements on the Sb (111) surface. We observe coherent phonon-induced binding-energy oscillations depending on momentum, band index, and phonon mode, highlighting the interplay of lattice and electronic degrees of freedom. We show that frozen-phonon DFT calculations can qualitatively reproduce the observed behavior, thereby reaffirming that the dynamics of electronic states modulated by weakly displaced coherent phonons are
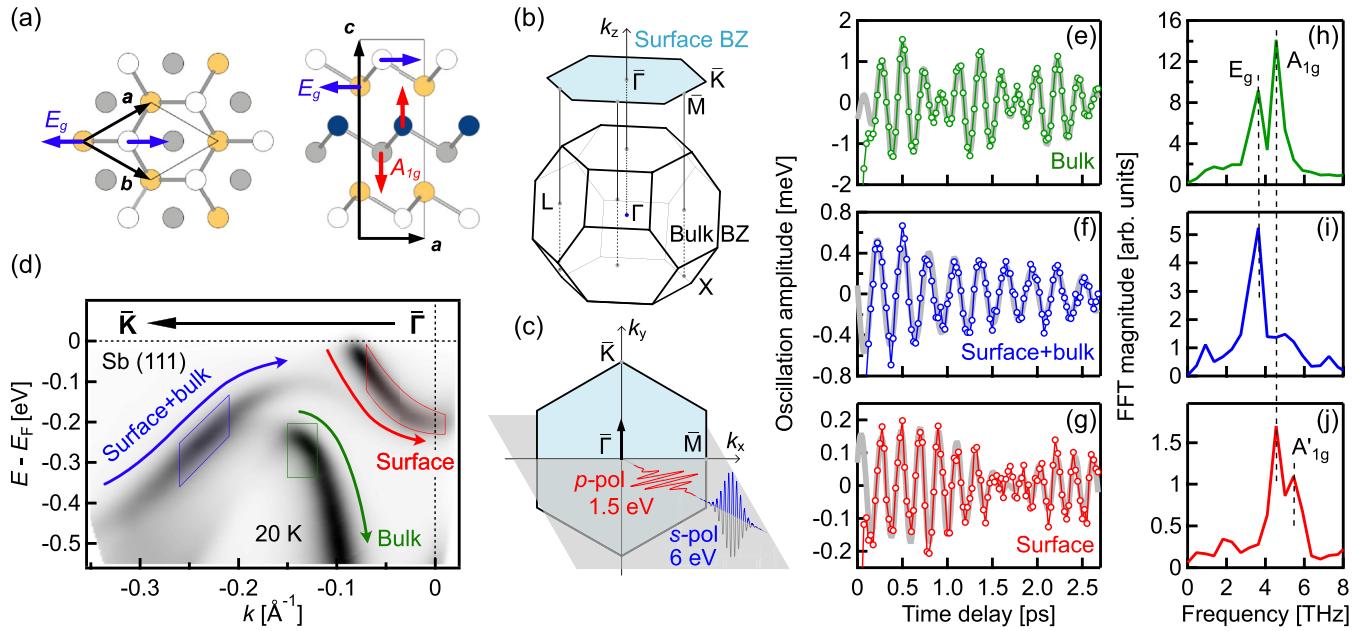
*shoya.sakamoto@issp.u-tokyo.ac.jp
†sobota@stanford.edu

FIG. 1. (a) Top and side views of the crystal structure of Sb. Blue and red arrows represent the atom displacement for the A_{1g} and E_g phonons, respectively. (b) Bulk and surface Brillouin zone of Sb. (c) Experimental geometry. (d) Equilibrium experimental angle-resolved photoemission spectroscopy (ARPES) spectrum along the $\overline{\Gamma}$-$\overline{K}$ direction. (e) and (h) Coherent phonon-induced binding-energy oscillations and the Fourier power spectra for the bulk band, (f) and (i) the surface + bulk band, and (g) and (j) the surface band, marked by green, blue, and red arrows in panel (d), respectively. The gray curves in panels (e)–(g) are fitted curves.

well described by the equilibrium concept of electron-phonon coupling.

Our trARPES setup is based on a Ti : sapphire regenerative amplifier outputting 1.5 eV, 35 fs pulses at a repetition rate of 312 kHz [26]. The photon energy was quadrupled to 6.0 eV for the probe pulse by two stages of second harmonic generation. The beam profiles for the pump and probe pulses were 68×85 and 38×41 μm^2 in full width at half maximum, respectively. The incident fluence of the 1.5 eV pump was 0.17 mJ/cm^2 and sufficiently weak to avoid a nonlinear response. Previous work found a 9 mJ/cm^2 threshold for frequency chirping [27], and >1 mJ/cm^2 leads to phonon softening in the similar semimetal Bi [28]. Photoelectrons were collected by a hemispherical analyzer, and spectra were recorded as a function of pump-probe delay. The overall time resolution was deduced to be 85 fs from cross-correlations of pump and probe pulses. The measurement temperature was 20 K. The light incidence plane was along the mirror plane of the sample, and the pump and probe light polarizations were p and s, respectively, as shown in Fig. 1(c). Photoelectrons are collected along the $\overline{\Gamma}$-$\overline{K}$ direction of the surface Brillouin zone as shown by a black arrow in Fig. 1(c). To detect weak coherent phonon oscillations, our accumulated data required correction of systematic drifts along the energy, momentum, and time axes, as described in the Supplemental Material [29].

First-principle calculations were performed on a 9 Sb bi-layer slab (18 Sb layers) with a 30 Å vacuum layer using the full-potential augmented-plane-wave method as implemented in the WIEN2K code [30]. Note that Sb bilayers become topological with $\geqslant$8 bilayers according to a previous DFT calculation [16]. The experimental lattice structure was used for the calculation. For the exchange-correlation potential, the generalized gradient approximation of the Perdew-Burke-

Ernzerhof parameterization [31] was employed with the spin-orbit interaction taken into account. The Brillouin zone integration was performed on a $20 \times 20 \times 1$ k-point mesh. We displaced Sb atoms by ±0.02, ±0.05, and $\pm0.1\%$ of the c-axis lattice constant (11.22 Å) along the trigonal axis for the A_{1g} phonon and by ±0.01, ±0.02, and $\pm0.05\%$ perpendicular to the trigonal axis for the E_g phonon. These displacement values result in binding-energy shifts that are resolvable while maintaining a linear relationship between the energy shift and the displacement [29]. The displacement directions for the A_{1g} and E_g phonons are depicted by red and blue arrows in Fig. 1(a), respectively. The band structures were calculated for each displacement, and the obtained binding-energy shift [$\Delta\varepsilon_n(k)$] as a function of atom displacement (Δr) was fitted by a linear function at each momentum to obtain the proportionality constant $\Delta\varepsilon/\Delta r$, which corresponds to the deformational potential. In this way, we could minimize and characterize errors from the DFT calculations [29].

Figure 1(d) shows the equilibrium ARPES spectrum taken along the $\overline{\Gamma}$-$\overline{K}$ direction. The spectrum is consistent with previous studies [18,32] and has three sharp energy bands marked by arrows in Fig. 1(d). The band marked by a green arrow is a bulk band, while the band marked by a red arrow is a surface band. The band marked by a blue arrow has surface character near $\overline{\Gamma}$ but has increasing bulk character as k increases (see the Supplemental Material for the orbital character of each band [29]). We thus refer to these three bands as the bulk band (green arrow), the surface band (red arrow), and the surface + bulk band (blue arrow) hereafter.

These surface and surface + bulk bands are Rashba-type spin-split bands [32,33]. However, unlike usual Rashba systems, the inner band (surface band) connects to the conduction band, while the outer band (surface + bulk band) connects

to the valence band, which is a manifestation of Sb being topologically nontrivial [14,17].

To examine the temporal evolution of the energy bands, we track the binding energy of each band by fitting a Gaussian function to the energy distribution curve (EDC) at each k-point and at each delay time. Figures 1(e)–1(g) show how the three bands oscillate in the binding energy as a function of delay time after the pump pulse. Here, fifth-order polynomial backgrounds are subtracted to extract the oscillatory components. For this figure, the oscillatory curves are averaged from $k = -0.15$ to -0.12 Å^{-1} for the bulk band, $k = -0.26$ to -0.21 Å^{-1} for the surface + bulk band, and $k = -0.07$ to 0.01 Å^{-1} for the surface band. These integration regions are indicated by boxes in Fig. 1(d). The bulk band shows the strongest average oscillation with an amplitude >1 meV. The surface + bulk band shows weaker oscillation than the bulk, and the surface band shows the weakest oscillation with an amplitude <0.2 meV. The weaker responses of the surface-related bands indicate that the electron-phonon coupling is weaker for the surface bands, as also suggested in Ref. [18].

Figures 1(h)–1(j) show the magnitude of the Fourier transforms of the curves shown in Figs. 1(e)–1(g). The Fourier transform of the bulk band oscillation has two peaks ~ 3.6 and 4.5 THz, which correspond to the E_g and A_{1g} phonon modes [34], respectively. The multifrequency oscillation can also be seen as a beating pattern in Fig. 1(e). The surface + bulk band does not show A_{1g} oscillations but shows E_g oscillation only. On the contrary, the surface band does not couple to the E_g phonon but couples to the A_{1g} phonon.

The surface band has an additional higher-frequency mode ~ 5.2 THz, which was predicted theoretically as a stiffening of the surface bilayer with respect to the bulk [25]. In this calculation, this manifests as a surface shear vertical mode with higher frequency (~ 5.1 THz) than the bulk A_{1g} mode (~ 4.8 THz). Therefore, we refer to this higher-frequency mode as the A'_{1g} mode. Our results corroborate association of the A'_{1g} mode with the surface because it is only present in the surface band and was absent in previous bulk-sensitive Raman spectroscopy [34] and time-resolved reflectivity (TRR) measurements [20]. A previous trARPES study [5] reported that Bi$_2$Se$_3$ also shows a mode associated with the surface state, the frequency of which is lower than that of the bulk A_{1g} mode. The opposite sign of the effect in these two materials suggests a difference in the nature of their interlayer atomic forces.

To be more quantitative, we perform a curve fit using two cosine functions with exponential decay, as shown below:

$$\Delta E = A_1 \cos(2\pi f_1 t + \phi_1)\exp\left(-\frac{t}{\tau_1}\right)$$
$$+ A_2 \cos(2\pi f_2 t + \phi_2)\exp\left(-\frac{t}{\tau_2}\right). \quad (1)$$

Here, ΔE denotes the shift of the binding energy, $f_{1,2}$ and $\phi_{1,2}$ denote the frequency and the phase of the oscillation, respectively, and $\tau_{1,2}$ represents the decay time. The fitting is performed for the delay time >0.2 ps. The fits are represented by gray curves in Figs. 1(e)–1(g), and they reproduce the data well. This agreement suggests that complex photoinduced forces and associated nonequilibrium carrier dynamics are settled after the first few hundred femtoseconds and that the

TABLE I. Fitting parameters for Eq. (1).

	Bulk		Surface + bulk	Surface	
	A_{1g}	E_g	E_g	A_{1g}	A'_{1g}
f (THz)	4.66(1)	3.49(1)	3.50(1)	4.66(2)	5.25(3)
A (meV)	0.89(4)	0.69(4)	0.60(5)	0.23(3)	0.04(1)
ϕ (π)	−0.68(2)	0.46(2)	0.45(3)	−0.41(4)	0.56(8)
$1/\tau$ (ps^{-1})	0.13(3)	0.23(4)	0.48(7)	0.8(2)	0.0(2)

subsequent sinusoidal oscillations reflect a quasi-equilibrium deformation potential that resembles the ground state. The deduced fitting parameters are summarized in Table I.

The fitted frequencies of the A_{1g} and E_g phonon modes are 4.66 ± 0.01 and 3.49 ± 0.01 THz, consistent with the frequencies of 4.67 (4.65) and 3.51 (3.47) THz observed in Raman spectroscopy (TRR) measurements [20,34]. This agreement confirms that the pump fluence is low enough to limit changes of the curvature of the interatomic potential to below detection threshold. The decay rates of A_{1g} and E_g phonons in the bulk band are 0.13 ± 0.03 and 0.23 ± 0.04 ps^{-1}, also comparable with the decay rates of 0.092 and 0.31 ps^{-1} observed in the TRR measurements [20]. Although the bulk band behaves consistently with the TRR measurement, the surface band and the surface + bulk band show faster decay, possibly suggesting increased dampening near the surface.

Figure 2 shows the momentum dependence of the band oscillation amplitudes and phases. Here, Eq. (1) was fitted to the EDC peak-position oscillation at each momentum with the decay rates and the frequencies fixed to the ones shown in Table I to minimize the number of free parameters. The surface + bulk band shows peculiar behavior: the phase rotates by π at $k = -0.3$ Å^{-1}. This behavior is reminiscent of antiphase oscillations reported in Bi$_2$Te$_3$ [6] and BaFe$_2$As$_2$ [35]. The present finding differs in that the pivoting occurs at a
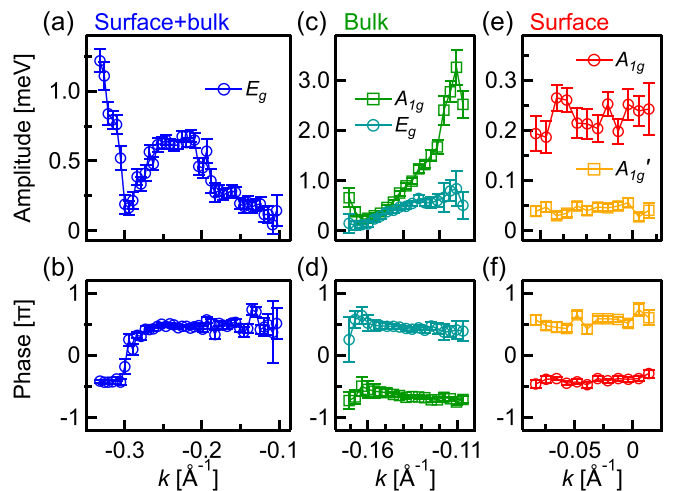

FIG. 2. Momentum dependence of (a) the binding-energy oscillation amplitudes and (b) phases for the surface + bulk band, (c) and (d) the bulk band, and (e) and (f) the surface band.
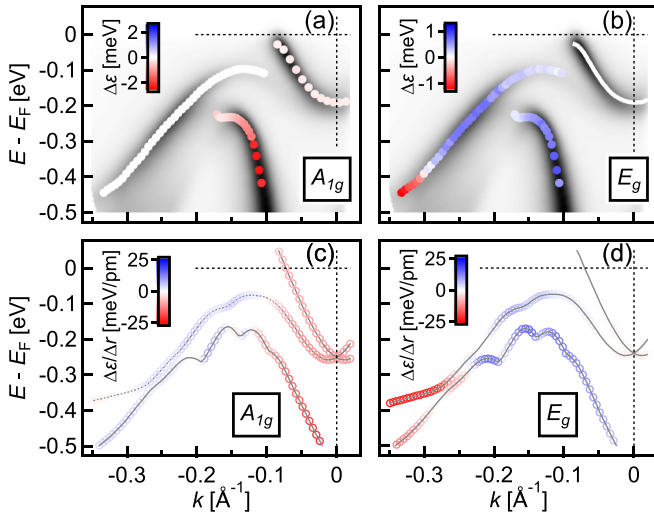
FIG. 3. (a) and (b) A_{1g} and E_g phonon oscillation amplitudes on each band at each momentum obtained in the experiments and (c) and (d) the density functional theory (DFT)-calculated deformation potentials. The oscillation amplitudes are represented by color.

seemingly arbitrary k-point and is not associated with high-symmetry directions in the Brillouin zone.

In contrast, the bulk band and the surface band exhibit nearly constant phases. The bulk band oscillations increase in amplitude approaching the $\overline{\Gamma}$ point [Fig. 2(c)], while the surface band oscillations show little momentum dependence in the measured range [Figs. 2(e) and 2(f)].

Figures 3(a) and 3(b) visualize the momentum- and band-dependent oscillation amplitudes for the A_{1g} and E_g phonon modes. Filled circles are plotted at the EDC peak positions, with their colors representing the signed oscillation amplitudes determined by multiplication with a phase factor, namely, $\Delta\varepsilon(k) = A(k) \times \sin[\phi(k)]$. The surface + bulk band reverses oscillation phase at $k \sim -0.3$ Å^{-1}. Because the E_g mode was not detected for the surface band, we use white solid markers for its peak position in Fig. 3(b).

To understand the momentum dependence of oscillation amplitudes and phases, we performed frozen-phonon DFT calculations and compared them with the experimental data. Figures 3(c) and 3(d) show the calculated deformation potential $\Delta\varepsilon/\Delta r$, plotted similarly to Figs. 3(a) and 3(b). DFT calculates a nonzero coupling for all modes and bands, and thus, the absence of certain modes in experiment does not signify that these mode couplings are symmetry forbidden [29].

For the A_{1g} mode, the surface + bulk band shows weak but finite response. In contrast to the experimental results, the surface and bulk bands show similar magnitudes of response; we speculate that the weak surface response in experiment may be attributed to a smaller surface bilayer distortion than the deeper layers because the surface bilayer is stiffer [25]. This speculation should be tested in future studies by directly measuring the atomic motion using time-resolved diffraction techniques [8,36,37], although it may be challenging to separately detect surface atom motion. Based on the calculated deformation potential, the A_{1g} atomic displacement Δr is

inferred to be ~0.03 pm for the surface bilayer, 0.1 pm for the bulk bilayers for 0.17 mJ/cm^2 incident pump fluence.

On the other hand, for the E_g mode, the calculation reproduced well the experimental observations: the surface + bulk band indeed shows a phase reversal around $k = -0.25$ Å^{-1}, and the surface band does not respond to the E_g displacement. The improved agreement for the E_g mode compared with the A_{1g} mode may be attributed to the fact that the E_g distortion is less sensitive to the surface termination since its displacement direction is parallel to the surface. The E_g atomic displacement Δr is inferred to be ~0.1 pm for both the surface and bulk bilayers for 0.17 mJ/cm^2 incident pump fluence. Despite these minor discrepancies, we find that the experimental data are qualitatively well described by the frozen-phonon DFT calculations. It is worth noting that the E_g phase reversal occurs where the two bands approach each other, and therefore, the reversal may be associated with their hybridization in this region.

Since the frozen-phonon calculations with equilibrium deformation potential reproduce the experimental observations well, we conclude that the band and momentum dependence of the deformation potential is not qualitatively modified by the pumping process, provided the excitation density is sufficiently low. Here, the pump pulse increases the electron temperature to 330 K, and the electron system cools to 130 K after 2.6 ps [29]. This perturbative excitation relaxes slowly compared with the period of the optical phonons, while the interatomic potentials remain practically indistinguishable from the ground state, as evident by the absence of a frequency chirp and agreement with Raman frequencies. In this regime, the pump is strong enough to launch coherent phonons but does not alter the deformation potential appreciably. Despite the excellent qualitative agreement, let us note again that it is necessary to determine the atomic displacement Δr for each atom to fully reveal the relationship between coherent phonon motion and resultant electronic structure dynamics in a quantitative manner, and such an investigation should be performed in future studies.

In summary, in this letter, we have revealed band-, momentum-, and phonon-mode-dependent electron-phonon coupling in Sb (111), which has been well reproduced by DFT calculations. It has been demonstrated that coherent phonons not only rigidly shift bands in energy but also exhibit a dependence on bulk/surface character as well as interband hybridizations. The fact that these behaviors are captured in frozen-phonon DFT calculations provides strong evidence that coherent phonon responses are rooted in the equilibrium concept of electron-phonon coupling. These results further justify the use of trARPES to investigate strongly correlated materials, in which the electron-phonon interactions are intrinsically intertwined with the effect of strong electron interactions.

[1] F. S. Khan and P. B. Allen, Phys. Rev. B **29**, 3341 (1984).

[2] U. De Giovannini, H. Hübener, S. A. Sato, and A. Rubio, Phys. Rev. Lett. **125**, 136401 (2020).

[3] E. Papalazarou, J. Faure, J. Mauchain, M. Marsi, A. Taleb-Ibrahimi, I. Reshetnyak, A. van Roekeghem, I. Timrov, N. Vast, B. Arnaud, and L. Perfetti, Phys. Rev. Lett. **108**, 256808 (2012).

[4] J. Faure, J. Mauchain, E. Papalazarou, M. Marsi, D. Boschetto, I. Timrov, N. Vast, Y. Ohtsubo, B. Arnaud, and L. Perfetti, Phys. Rev. B **88**, 075120 (2013).

[5] J. A. Sobota, S.-L. Yang, D. Leuenberger, A. F. Kemper, J. G. Analytis, I. R. Fisher, P. S. Kirchmann, T. P. Devereaux, and Z.-X. Shen, Phys. Rev. Lett. **113**, 157401 (2014).

[6] E. Golias and J. Sánchez-Barriga, Phys. Rev. B **94**, 161113(R) (2016).

[7] L. Rettig, S. O. Mariager, A. Ferrer, S. Grübel, J. A. Johnson, J. Rittmann, T. Wolf, S. L. Johnson, G. Ingold, P. Beaud, and U. Staub, Phys. Rev. Lett. **114**, 067402 (2015).

[8] S. Gerber, S.-L. Yang, D. Zhu, H. Soifer, J. Sobota, S. Rebec, J. J. Lee, T. Jia, B. Moritz, C. Jia, A. Gauthier, Y. Li, D. Leuenberger, Y. Zhang, L. Chaix, W. Li, H. Jang, J.-S. Lee, M. Yi, G. L. Dakovski, S. Song, J. M. Glownia, S. Nelson, K. W. Kim, Y.-D. Chuang, Z. Hussain, R. G. Moore, T. P. Devereaux, W.-S. Lee, P. S. Kirchmann, and Z.-X. Shen, Science **357**, 71 (2017).

[9] S.-L. Yang, J. A. Sobota, Y. He, D. Leuenberger, H. Soifer, H. Eisaki, P. S. Kirchmann, and Z.-X. Shen, Phys. Rev. Lett. **122**, 176403 (2019).

[10] T. Suzuki, Y. Shinohara, Y. Lu, M. Watanabe, J. Xu, K. L. Ishikawa, H. Takagi, M. Nohara, N. Katayama, H. Sawa, M. Fujisawa, T. Kanai, J. Itatani, T. Mizokawa, S. Shin, and K. Okazaki, Phys. Rev. B **103**, L121105 (2021).

[11] P. Hein, S. Jauernik, H. Erk, L. Yang, Y. Qi, Y. Sun, C. Felser, and M. Bauer, Nat. Commun. **11**, 2613 (2020).

[12] J. J. Li, J. Chen, D. A. Reis, S. Fahy, and R. Merlin, Phys. Rev. Lett. **110**, 047401 (2013).

[13] S. M. O'Mahony, F. Murphy-Armando, E. D. Murray, J. D. Querales-Flores, I. Savić, and S. Fahy, Phys. Rev. Lett. **123**, 087401 (2019).

[14] D. Hsieh, Y. Xia, L. Wray, D. Qian, A. Pal, J. Dil, J. Osterwalder, F. Meier, G. Bihlmayer, C. Kane, Y. Hor, R. Cava, and M. Hasan, Science **323**, 919 (2009).

[15] J. Seo, P. Roushan, H. Beidenkopf, Y. S. Hor, R. J. Cava, and A. Yazdani, Nature (London) **466**, 343 (2010).

[16] P. Zhang, Z. Liu, W. Duan, F. Liu, and J. Wu, Phys. Rev. B **85**, 201410(R) (2012).

[17] G. Bian, T. Miller, and T.-C. Chiang, Phys. Rev. Lett. **107**, 036802 (2011).

[18] Z.-J. Xie, S.-L. He, C.-Y. Chen, Y. Feng, H.-M. Yi, A.-J. Liang, L. Zhao, D.-X. Mou, J.-F. He, Y.-Y. Peng, X. Liu, Y. Liu, G.-D. Liu, X.-L. Dong, L. Yu, J. Zhang, S.-J. Zhang, Z.-M. Wang, F.-F. Zhang, F. Yang, Q.-J. Peng, X.-Y. Wang, C.-T. Chen, Z.-Y. Xu, and X.-J. Zhou, Chin. Phys. Lett. **31**, 067305 (2014).

[19] T. K. Cheng, S. D. Brorson, A. S. Kazeroonian, J. S. Moodera, G. Dresselhaus, M. S. Dresselhaus, and E. P. Ippen, Appl. Phys. Lett. **57**, 1004 (1990).

[20] K. Ishioka, M. Kitajima, and O. V. Misochko, J. Appl. Phys. **103**, 123505 (2008).

[21] H. J. Zeiger, J. Vidal, T. K. Cheng, E. P. Ippen, G. Dresselhaus, and M. S. Dresselhaus, Phys. Rev. B **45**, 768 (1992).

[22] G. A. Garrett, T. F. Albrecht, J. F. Whitaker, and R. Merlin, Phys. Rev. Lett. **77**, 3661 (1996).

[23] T. E. Stevens, J. Kuhl, and R. Merlin, Phys. Rev. B **65**, 144304 (2002).

[24] Y. Shinohara, S. A. Sato, K. Yabana, J.-I. Iwata, T. Otobe, and G. F. Bertsch, J. Chem. Phys. **137**, 22A527 (2012).

[25] D. Campi, M. Bernasconi, and G. Benedek, Phys. Rev. B **86**, 075446 (2012).

[26] A. Gauthier, J. A. Sobota, N. Gauthier, K.-J. Xu, H. Pfau, C. R. Rotundu, Z.-X. Shen, and P. S. Kirchmann, J. Appl. Phys. **128**, 093101 (2020).

[27] O. V. Misochko, M. Hase, K. Ishioka, and M. Kitajima, Phys. Rev. Lett. **92**, 197401 (2004).

[28] D. M. Fritz, D. A. Reis, B. Adams, R. A. Akre, J. Arthur, C. Blome, P. H. Bucksbaum, A. L. Cavalieri, S. Engemann, S. Fahy, R. W. Falcone, P. H. Fuoss, K. J. Gaffney, M. J. George, J. Hajdu, M. P. Hertlein, P. B. Hillyard, M. Horn-von Hoegen, M. Kammler, J. Kaspar, R. Kienberger, P. Krejcik, S. H. Lee, A. M. Lindenberg, B. McFarland, D. Meyer, T. Montagne, É. D. Murray, A. J. Nelson, M. Nicoul, R. Pahl, J. Rudati, H. Schlarb, D. P. Siddons, K. Sokolowski-Tinten, Th. Tschentscher, D. von der Linde, and J. B. Hastings, Science **315**, 633 (2007).

[29] See Supplemental Material at http://link.aps.org/supplemental/10.1103/PhysRevB.105.L161107 for details of data analyses, electron tempeature estimation, atomic and orbital characters of the energy bands, the method to extract deformation potential, and symmetry discussion for electron-phonon coupling.

[30] P. Blaha, K. Schwarz, G. K. H. Madsen, D. Kvasnicka, J. Luitz, R. Laskowski, F. Tran, and L. D. Marks, WIEN2K, an augmented plane wave + local orbitals program for calculating crystal properties (Karlheinz Schwarz, Vienna University of Technology, Austria, 2018).

[31] J. P. Perdew, K. Burke, and M. Ernzerhof, Phys. Rev. Lett. **77**, 3865 (1996).

[32] K. Sugawara, T. Sato, S. Souma, T. Takahashi, M. Arai, and T. Sasaki, Phys. Rev. Lett. **96**, 046411 (2006).

[33] A. Takayama, T. Sato, S. Souma, and T. Takahashi, New J. Phys. **16**, 055004 (2014).

[34] X. Wang, K. Kunc, I. Loa, U. Schwarz, and K. Syassen, Phys. Rev. B **74**, 134305 (2006).

[35] K. Okazaki, H. Suzuki, T. Suzuki, T. Yamamoto, T. Someya, Y. Ogawa, M. Okada, M. Fujisawa, T. Kanai, N. Ishii, J. Itatani, M. Nakajima, H. Eisaki, A. Fujimori, and S. Shin, Phys. Rev. B **97**, 121107(R) (2018).

[36] M. Greif, L. Kasmi, L. Castiglioni, M. Lucchini, L. Gallmann, U. Keller, J. Osterwalder, and M. Hengsberger, Phys. Rev. B **94**, 054309 (2016).

[37] L. Waldecker, T. Vasileiadis, R. Bertoni, R. Ernstorfer, T. Zier, F. H. Valencia, M. E. Garcia, and E. S. Zijlstra, Phys. Rev. B **95**, 054302 (2017).